SAND2014-18554C

# Ampair 600 Wind Turbine 3-Bladed Assembly Substructuring using the Transmission Simulator Method

**Daniel R. Roettgen & Randy L. Mayes**
*Experimental Mechanics, NDE, and Model Validation Department*
*Sandia National Laboratories**
*P.O. Box 5800 – MS 0557*
*Albuquerque, NM 87185*
droettgen@wisc.edu
rlmayes@sandia.gov

* Sandia National Laboratories is a multi-program laboratory managed and operated by Sandia Corporation, a wholly owned subsidiary of Lockheed Martin Corporation, for the U.S. Department of Energy's National Nuclear Security Administration under contract DE-AC04-94AL85000.

**ABSTRACT**

This paper contains an example of the transmission simulator method for experimental dynamic substructuring using the Ampair 600 Wind Turbine. The structure of interest is the hub-and-three-bladed assembly. A single blade and hub is used as a substructure to develop a model for the hub-and-three-bladed assembly. The single-blade-and-hub substructure was developed from elastic modes of a free-free test and rigid body modes analytically derived from measured mass properties. This substructure can be rotated and replicated using the hub as a transmission simulator. Substructuring calculations were then performed using the transmission simulator method to derive a model of the hub-and-three-bladed assembly. This paper concludes with a comparison for this combined model to truth data derived from a free-free modal test of the entire rotor.

**Keywords:** Experiment; MCFS; Dynamic Substructuring; Transmission Simulator; Wind Turbine

## 1. Introduction

As manufactured systems become more complex a need for advanced analytical tools to analyze these systems becomes a necessity. Dynamic substructuring allows an analyst to predict the dynamic response of a complex system by analyzing or testing subcomponents. Thus, if subcomponents can be modeled or tested, the result for a full model can be predicted and these subcomponents can be modified to help mature the design. Experimental substructuring is particularly useful when a system is too large to test as an assembly, or when subcomponent hardware is available but the detailed design definition is not (for example, for a subcomponent produced by an outside company). This paper contains a detailed example of dynamic substructuring on the Ampair 600 Wind Turbine test bed. The goal of this exercise is to construct the dynamics of a three-bladed rotor experiment using the results from a single-blade-and-hub experiment. To complete this exercise, two experiments were performed. The first was a hub-and-three-bladed experiment that will be used as a truth model. The second was the testing of the subcomponent containing one blade and the rotor hub. In addition to the details of these experiments, this paper contains the substructuring methodology and some simple experimental checks used to help ensure the quality of the data that was taken experimentally. For this exercise the transmission simulator method was used.

Advantages of the transmission simulator method can be found in [1]. Here we focus on a few of the advantages for this application. The transmission simulator method is often used over more traditional substructuring methods when it is difficult to simulate the boundary conditions between individual pieces of a system. By using the hub as the transmission simulator two key advantages are gained. One is that the compliance and the damping of the joint connecting the blade and hub are captured. The second is that the hub mass loads the root of the blade so that blade stiffness at the root is appropriately exercised. Often a similar fixture is used as a transmission simulator, but for this exercise the actual part was used because it was readily available and was certain to simulate the interface conditions correctly. This provides the best possible simulation of the blade-to-hub joint as the actual joint dynamics are contained within the experiment.

## 2. Test Objective and Methods

The objective for this exercise is to generate a dynamic model of the hub-and-three-bladed system, pictured in Figure 1, from the Ampair 600 Wind Turbine using the transmission simulator method. This model will be compared to a "truth model" that was derived from a modal test of the pictured assembly. Previous tests containing these structures in similar configurations [2-4] show that the highest frequencies of interest would occur below 175 Hz, and thus the test range was set to 200 Hz for the truth model to allow the modes of interest (and a few higher) to be captured. For each test, a PCB 086C05 impact hammer was used to excite the structures' elastic modes. In an attempt to minimize non-linearities in the system, the output of the hammer was amplified allowing extremely soft taps to be used during testing. The auto spectrum of this input was monitored during testing to ensure quality data was gathered. After completing the modal testing, modes were extracted from the experimental data using the SMAC algorithm [5].

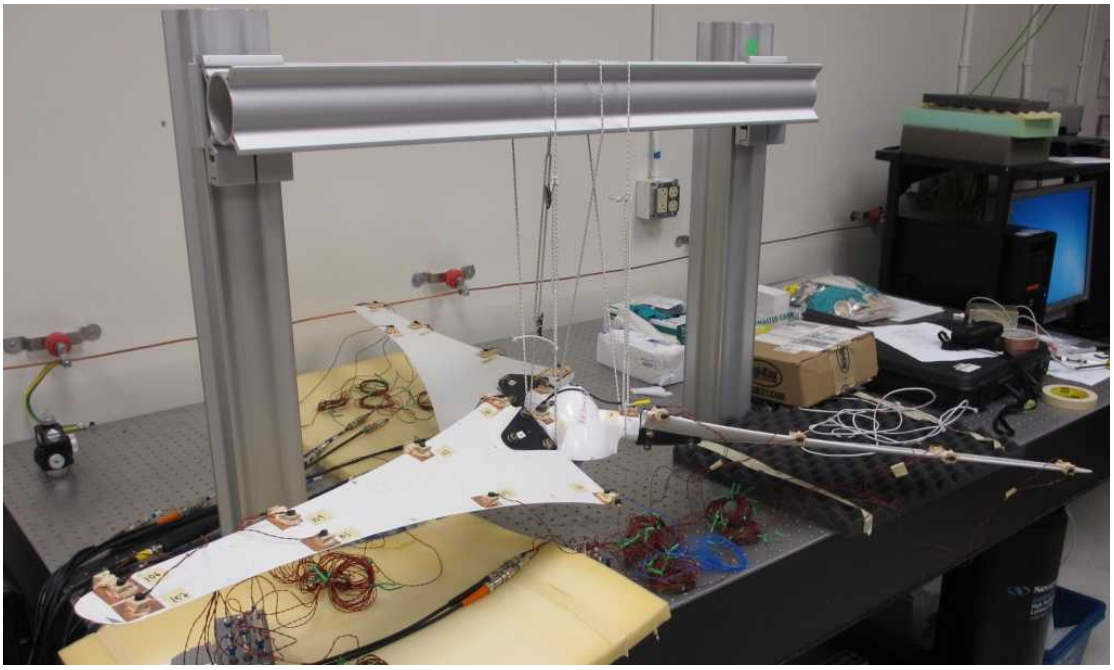

**Figure 1. Wind Turbine Truth Assembly**

Tests were performed on two different structures in order to create both a full-assembly "truth" model and a sub-assembly "substructure" model that could be replicated and assembled into the complete hub-and-three-bladed assembly. The first structure was the hub connected to all three blades. Hardware assets were used from Sandia National Laboratories with the serial numbers for Blades A, B, and C being SNL009, SNL008, and SNL007, respectively. The second structure tested was the turbine hub assembly with just Blade A connected. The results from the substructure test will be replicated (and rotated) two times, so two additional hubs will need to be subtracted as they are the common piece being used as a transmission simulator.

Each third of the turbine was given its own Cartesian coordinate system with $x$ along the blade, $y$ perpendicular to $x$ in the rotation plane, and $z$ along the axis of rotation. The origin of these coordinates systems was defined at a common point on the center of the hub. Figure 2 shows these coordinate systems as they are aligned with each blade.

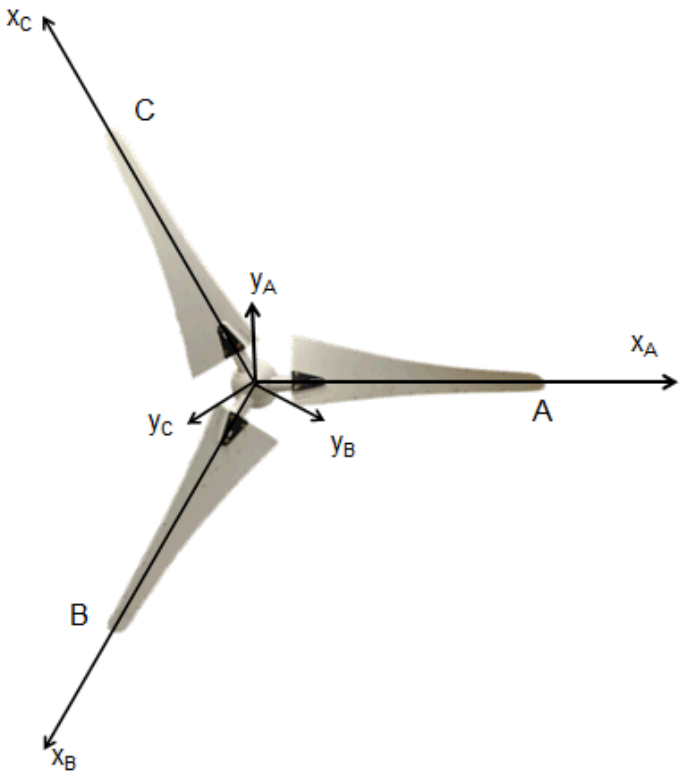


**Figure 2. Wind Turbine Coordinate System – Truth Test**

## 2.1 Hub-and-Three-Bladed Test (Truth Test)

### 2.1.1 Test Set-Up

The hub-and-three-bladed assembly was instrumented with 36 single axis accelerometers as well as 3 triaxial accelerometers. The primary blade (Blade A) was instrumented based on previous testing [2,3] such that all mode shapes up to the third out-of-plane bending mode would be independent. This primary blade was instrumented more heavily than the secondary blades as this instrumentation would remain in place to capture data during the subcomponent testing. Accelerometer locations and directions are depicted in Figure 3.

Two 2250AM1-10 uniaxial accelerometers with a sensitivity of 10 mV/g were placed at 4 locations along the leading edge of each blade. These accelerometers were oriented with the *y* and *z* directions for each blade's local coordinate system. Accelerometers were also placed along the trailing edge of the blade but mainly oriented in the *z* direction with one accelerometer placed in the *y* direction at the trailing edge root of each blade.

The hub was instrumented with three tri-axial Endevco 65-100 accelerometers with a higher sensitivity of 100 mV/g. This higher sensitivity was required because hub motion tended to be very small compared to the light flexible blades. These tri-axial accelerometer was placed on the branch extending from the hub associated with each blade. Additionally, one 100 mV/g uniaxial PCB 352/A-24 accelerometer was placed on the Blade A third of the hub pointed in the *y* direction

Blocks were used to align the accelerometers in the local blade displacement coordinate systems with accelerometers on the blade face pointing in the *z* direction and those on the trailing and leading edge in the *y* direction. These wood blocks were taken into account when analytically constructing rigid body modes for the different assemblies.

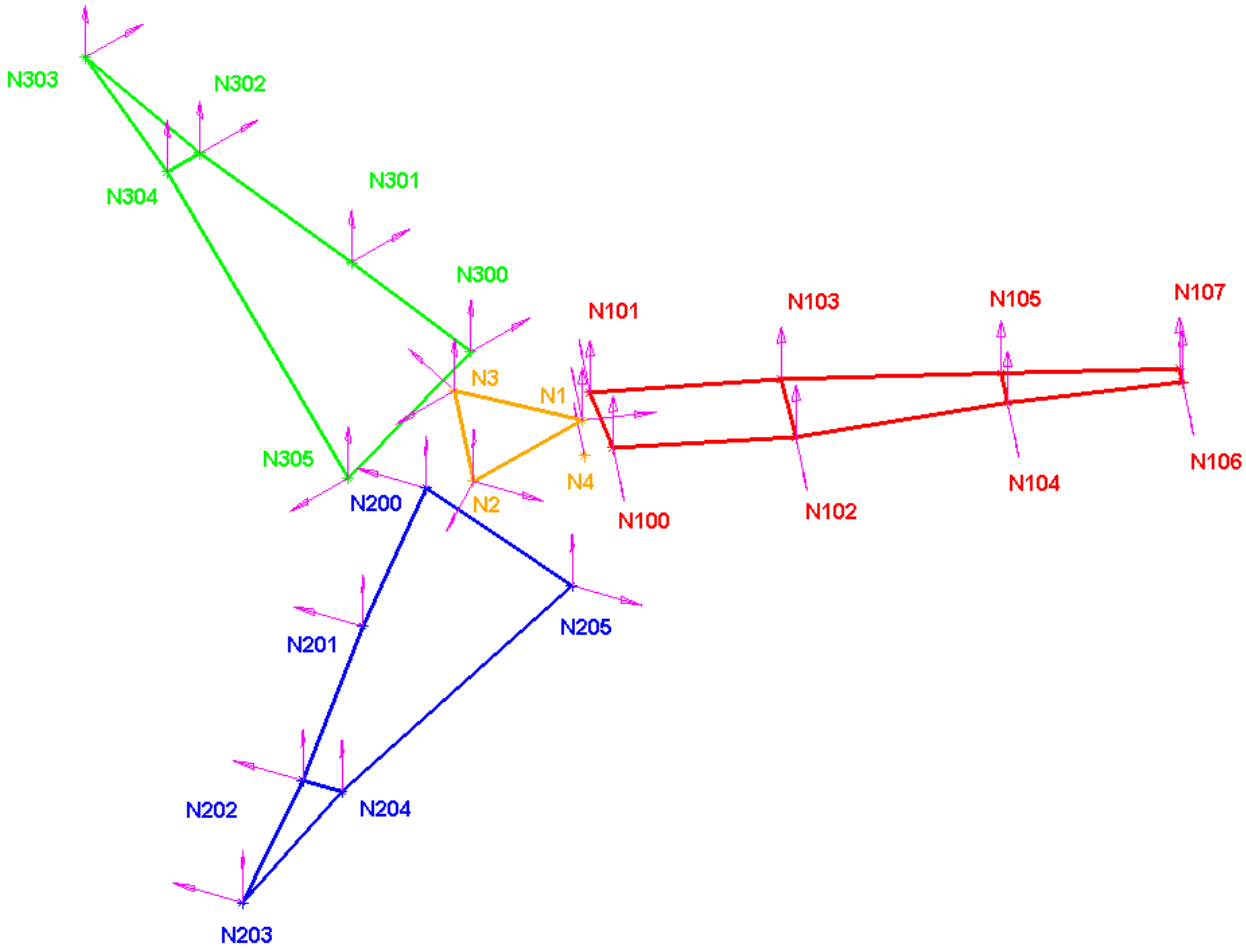


**Figure 3. Truth Model Assembly (left) Instrumentation Placement (right)**

The hub-and-three-bladed assembly was suspended from a structure on an optical table using bungee cords to simulate a free-free condition as seen in Figure 1. Previous work showed the lowest elastic mode to occur at about 20 Hz. In an effort to minimize error due to the boundary conditions, the bungee cords provided a rigid body bounce mode around 2 Hz. This achieved a desired ratio of 10 times in order to minimize frequency error due to boundary conditions as discussed in [6].

Analytical rigid body mode shapes were calculated using the moments of inertia and center of gravity detailed in [3]. With the larger number of accelerometers (and positioning blocks), it was decided that the mass of these items was not negligible in the calculation of the mass properties. These blocks were accounted for when calculating the mass properties used to determine rigid body modes. The mass properties are listed in Table 1.

| | **Entire Rotor** |
|---|---|
| Mass | 6.29 kg |
| $cg_x$ | 0.00 m |
| $cg_y$ | 0.00 m |
| $cg_z$ | -0.0673 m |
| $I_{xx}$ | 0.221 kg-m$^2$ |
| $I_{yy}$ | 0.224 kg-m$^2$ |
| $I_{zz}$ | 0.441 kg-m$^2$ |

**Table 1. Mass Properties for Hub-and-Three-Bladed System**

The suspended structure was excited at several drive points in the usual attempt to find the best location to excite each individual mode. Drive points were gathered on the blades and on the rotor hub. The drive points on the rotor hub provided the best results, not because they excited the modes the most, but because they excited the modes well enough and produced FRFs with the most linear characteristics. To create a truth model for the hub-and-three-bladed assembly, the measured response from the best was used to calculate the modal parameters for each elastic mode. Modes 7, 8, 9, 12, and 15 were derived from excitations with a drive point at node 1 in the *z* direction; while modes 10 and 11 were derived from excitations at node 4 in the *y* direction, and modes 13 and 14 were derived from excitations at node 3 in the *z* direction.

### 2.1.2 Results

The analytically generated rigid body modes were combined with 9 elastic modes extracted from the impact tests. These modes are detailed in Table 2. Light hammer excitations were used in an attempt to avoid non-linarites due to the jointed connection. Of particular note, modes 10 and 11 (elastic modes 4 and 5) exhibited a great deal of non-linearity and were particularity sensitive to the input force levels. Complex modal indicator functions (CMIFs) are shown for each of the drive points in Figure 4. Note that no single reference excites all modes well. Red circles in the figure show which modes were selected from each reference. We recognize that this truth test is only one realization of truth, since there is definitely variability in individual blades as well as the clearances in the hub brackets holding the blades.

| Mode | Frequency (Hz) | Damping Ratio ζ [%] | Description | Drive Point |
|---|---|---|---|---|
| 1 | 0.00 | 1.00% | *x* direction translation | Analytical |
| 2 | 0.00 | 1.00% | *y* direction translation | Analytical |
| 3 | 0.00 | 1.00% | *z* direction translation | Analytical |
| 4 | 0.00 | 1.00% | rotation about *x* | Analytical |
| 5 | 0.00 | 1.00% | rotation about *y* | Analytical |
| 6 | 0.00 | 1.00% | rotation about *z* | Analytical |
| 7 | 20.56 | 1.00% | 1st Bending, 3 Blades in Phase | 1Z |
| 8 | 27.78 | 0.98% | 1st Bending, Blade C out of Phase | 1Z |
| 9 | 29.03 | 0.87% | 1st Bending, Blade B out of Phase | 1Z |
| 10 | 61.10 | 1.71% | Edge-wise Mode, Blade C out of phase | 4Y |
| 11 | 64.29 | 1.27% | Edge-wise Mode, Blade B out of phase | 4Y |
| 12 | 70.68 | 1.11% | 2nd Bending, 3 Blades in Phase | 1Z |
| 13 | 99.40 | 1.48% | 2nd Bending, Blade C out of Phase | 3Z |
| 14 | 102.95 | 1.08% | 2nd Bending, Blade B out of Phase | 3Z |
| 15 | 155.00 | 1.33% | 3rd Bending, 3 Blades in Phase | 1Z |

**Table 2. List of extracted and analytically calculated modes from the hub-and-three-bladed test**

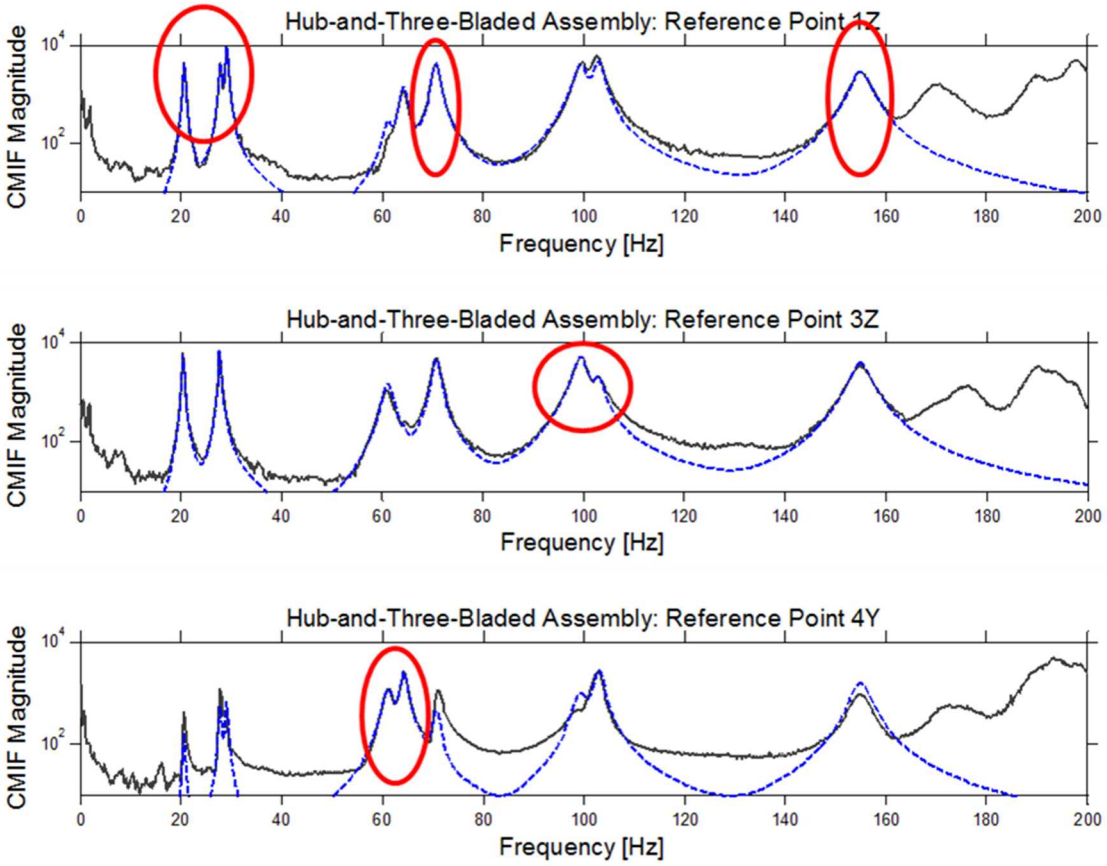


**Figure 4. CMIFs for Truth Model (Blue) and Drive Point Measurements (Black). Drive points: 1Z (top), 3Z (middle), 4Y (bottom)**

## 2.2 Single-Blade-and-Hub Test (Substructure Test)

### 2.2.1 Test Set-Up

With one realization of a truth model established, the next test to be completed was the single-blade-and-hub test. Blades B and C were removed from the hub leaving Blade A. The accelerometers on Blade A were not removed to preserve their location relative to the hub-and-three-bladed testing. The same impact hammer and instrumentation set-up were used for Blade A and the hub. Measurements were taken up to 200 Hz in order to capture up to the first three out-of-plane bending modes. The test set-up for the single-blade-and-rotor-hub system can be seen in Figure 5.

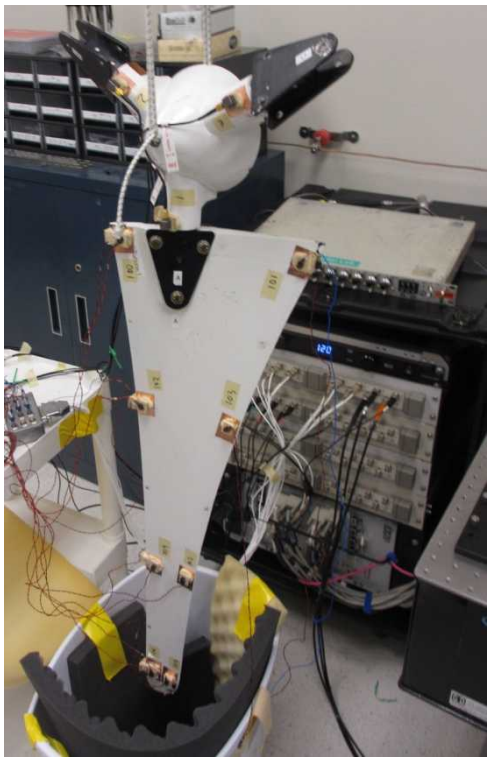

**Figure 5. Single-Blade-and-Rotor-Hub Experimental Set-Up**

Mass properties of the substructure were calculated using geometry and assumed symmetry properties of the hub-and-three-bladed system. Analytical rigid body modes were again calculated using the mass properties of the system. Substructure moments of inertia were calculated based on geometry and symmetry conditions and are shown in Table 3. The instrumentation blocks located on the single-blade-and-hub assembly were accounted for in these calculations.

| | **Single-Blade-and--Hub Assembly** |
|---|---|
| Mass | 4.52 kg |
| $cg_x$ | 0.0756 m |
| $cg_y$ | 0.000 m |
| $cg_z$ | -0.0632 m |
| $I_{xx}$ | 0.0252 kg-m$^2$ |
| $I_{yy}$ | 0.0972 kg-m$^2$ |
| $I_{zz}$ | 0.1414 kg-m$^2$ |

**Table 3. Mass Properties for** Single-Blade-and--Hub **System**

The subsystem was similarly tested at several drive points in order to determine the excitation locations that provided the best data for the subsystem's elastic modes. Modes 7, 8, 9, and 11 were derived from excitations at drive point location 3 in the *z* direction while mode 10 was derived from drive point location 4 in the *y* direction.

### 2.2.2 Results

The six analytically generated rigid body modes were combined with 5 elastic modes extracted from the impact tests. These modes are detailed in Table 4. Again, each elastic mode was selected from the strongest responding drive point. CMIFs for those selected drive points can be seen in Figure 6. Hammer strikes in the z-direction were found to easily excite bending and torsional modes while a *y* direction strike was again required to excite the blade in edgewise motion. The modes extracted from each reference are circled in red.

| Mode | Frequency (Hz) | Damping Ratio ζ [%] | Description | Drive Point |
|---|---|---|---|---|
| 1 | 0.00 | 1.00% | *x* direction translation | Analytical |
| 2 | 0.00 | 1.00% | *y* direction translation | Analytical |
| 3 | 0.00 | 1.00% | *z* direction translation | Analytical |
| 4 | 0.00 | 1.00% | Rotation about *x* | Analytical |
| 5 | 0.00 | 1.00% | Rotation about *y* | Analytical |
| 6 | 0.00 | 1.00% | Rotation about *z* | Analytical |
| 7 | 29.84 | 0.91% | 1st Bending | 3Z |
| 8 | 86.75 | 0.92% | 2nd Bending | 3Z |
| 9 | 149.82 | 1.51% | Edgewise Motion | 3Z |
| 10 | 178.25 | 2.62% | 1st Torsion | 4Y |
| 11 | 195.10 | 1.30% | 3rd Bending | 3Z |

**Table 4. List of extracted and analytically calculated modes from the single-blade-and-hub test**

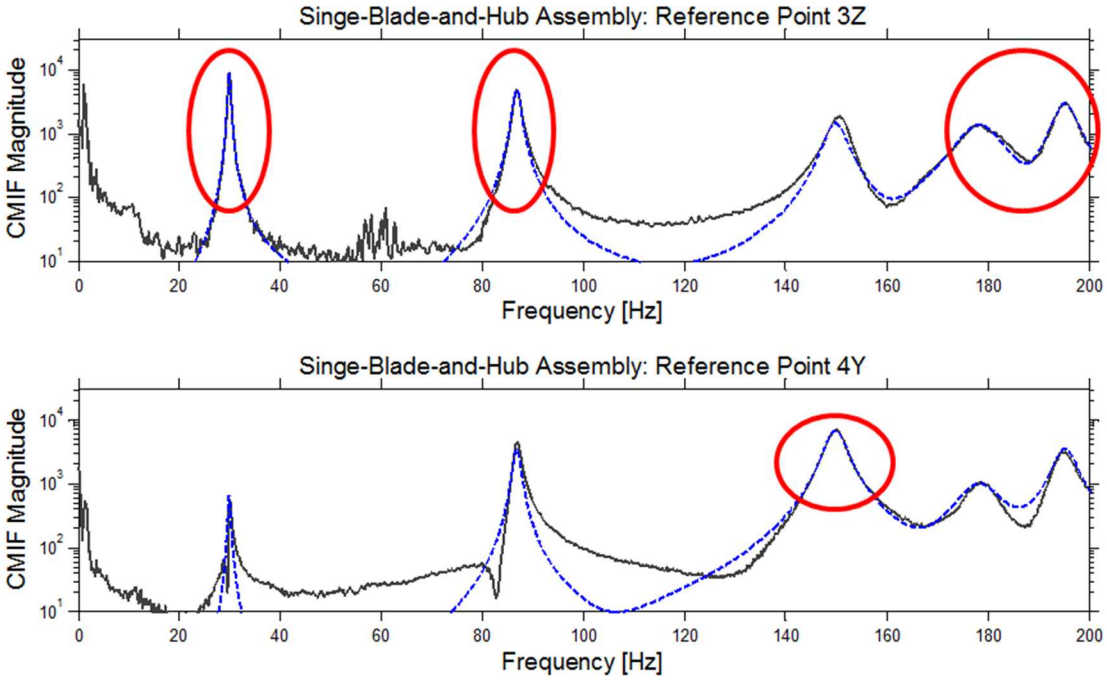


**Figure 6. CMIFs for Substructure Model (Blue) and Drive Point Measurements (Black). Drive points: 3Z (top), 4Y (bottom)**

## 3. Substructuring Methodology

The transmission simulator method was utilized in order to assemble the single-blade-and-hub into the full system. The rotor hub was used as the transmission simulator fixture. Three copies of the subsystem were rotated and added together linking the rotated degrees of freedom associated with the tri-axial accelerometers located on the rotor hub (transmission simulator). With three copies of the substructure included, two analytical copies of the transmission simulator needed to be subtracted out of the combined system to achieve the proper results for the mass of the hub.

The same rotor hub was used as a transmission simulator in a past experiment and was found to have a first elastic natural frequency above 1200 Hz [3]. This first elastic mode is far beyond the scope of the current test so only the rigid body modes of the transmission simulator will be used to couple the systems.

For the following calculations, the subscript *A* represents the first blade, Blade A, with *B*, and *C* representing the second and third blade respectively; the subscript *TS* represents the transmission simulator (rotor hub). The modal parameters $\omega$ and $\zeta$ represent the natural frequencies and damping ratios of their respective subsystems and $\Phi$ represents the associated mode shapes. The physical degrees of freedom are represented by vectors denoted *x* and the modal degrees of freedom are denoted

by vectors $q$. To begin, the system of equations is written in the standard mass-normalized modal representation of the equations of motion.

$$\begin{bmatrix} I_A & 0 & 0 & 0 \\ 0 & I_B & 0 & 0 \\ 0 & 0 & I_C & 0 \\ 0 & 0 & 0 & -2I_{TS} \end{bmatrix} \begin{Bmatrix} \ddot{q}_A \\ \ddot{q}_B \\ \ddot{q}_C \\ \ddot{q}_{TS} \end{Bmatrix} + \begin{bmatrix} 2\zeta_A\omega_A & 0 & 0 & 0 \\ 0 & 2\zeta_B\omega_B & 0 & 0 \\ 0 & 0 & 2\zeta_C\omega_C & 0 \\ 0 & 0 & 0 & -4\zeta_{TS}\omega_{TS} \end{bmatrix} \begin{Bmatrix} \dot{q}_A \\ \dot{q}_B \\ \dot{q}_C \\ \dot{q}_{TS} \end{Bmatrix} +$$

$$\begin{bmatrix} \omega_A{}^2 & 0 & 0 & 0 \\ 0 & \omega_B{}^2 & 0 & 0 \\ 0 & 0 & \omega_C{}^2 & 0 \\ 0 & 0 & 0 & -2\omega_{TS}{}^2 \end{bmatrix} \begin{Bmatrix} q_A \\ q_B \\ q_C \\ q_{TS} \end{Bmatrix} = \begin{Bmatrix} \Phi_A^T F_A \\ \Phi_B^T F_B \\ \Phi_C^T F_C \\ 2\Phi_{TS}^T F_{TS} \end{Bmatrix} \tag{1}$$

The physical constraints can be assembled equating the motion of each subsystem with that or the transmission simulator. This equation only applies to the subset of degrees of freedom which act to connect the transmission simulator between substructures.

$$\begin{bmatrix} I & 0 & 0 & -I \\ 0 & I & 0 & -I \\ 0 & 0 & I & -I \end{bmatrix} \begin{Bmatrix} x_A \\ x_B \\ x_C \\ x_{TS} \end{Bmatrix} = \begin{Bmatrix} 0 \\ 0 \\ 0 \\ 0 \end{Bmatrix} \tag{2}$$

The constraint equation can then be rewritten as modal coordinates as seen in Equation 3.

$$\begin{bmatrix} \Phi_A & 0 & 0 & -\Phi_{TS} \\ 0 & \Phi_B & 0 & -\Phi_{TS} \\ 0 & 0 & \Phi_C & -\Phi_{TS} \end{bmatrix} \begin{Bmatrix} q_A \\ q_B \\ q_C \\ q_{TS} \end{Bmatrix} = \begin{Bmatrix} 0 \\ 0 \\ 0 \\ 0 \end{Bmatrix} \tag{3}$$

In order to take advantage of the transmission simulator method, the constraints are now pre-multiplied by the pseudo-inverse of the transmission simulator mode shapes partitioned to the constraint degrees of freedom.

$$\begin{bmatrix} \Phi_{TS}^+ & 0 & 0 \\ 0 & \Phi_{TS}^+ & 0 \\ 0 & 0 & \Phi_{TS}^+ \end{bmatrix} \begin{bmatrix} \Phi_A & 0 & 0 & -\Phi_{TS} \\ 0 & \Phi_B & 0 & -\Phi_{TS} \\ 0 & 0 & \Phi_C & -\Phi_{TS} \end{bmatrix} \begin{Bmatrix} q_A \\ q_{Bc} \\ q_C \\ q_{TS} \end{Bmatrix} = \begin{Bmatrix} 0 \\ 0 \\ 0 \\ 0 \end{Bmatrix} \tag{4}$$

The two leading matrices can now be collected to form a single matrix, $A$, that contains the constraints for the modal degrees of freedom.

$$A \begin{Bmatrix} q_A \\ q_B \\ q_C \\ q_{TS} \end{Bmatrix} = A\{q\} = 0 \tag{5}$$

These constrained modal degrees of freedom can be transformed by some matrix, $L$, into a set of unconstrained generalized coordinates, $q_g$.

$$\{q\} = L\{q_g\} \tag{6}$$

Using this substitution requires that $L$ reside in the null space of $A$ because $q_g = 0$ would be a trivial solution. This means that L must be orthogonal to $A$ to fulfill Equation 5.

$$AL\{q_g\} = 0 \tag{7}$$

This substitution is then used in Equation 1 which is also pre-multiplied by $AL^T$ resulting in the coupled equations of motion for the system. The modal properties for this system can then be found as the modal properties for the new analytically substructured system. A final transform is then used to bring the solution for the modal degrees of freedom back into the physical domain. Note the $M$, $C$ and $K$ are defined as shown in Equation 1.

$$\overline{M}\ddot{q}_g + \overline{C}\dot{q}_g + \overline{K}q_g = 0$$

$$\overline{M} = L^T ML \qquad \overline{C} = L^T CL \qquad \overline{K} = L^T KL$$

$$x = \begin{bmatrix} \Phi_A & 0 & 0 & 0 \\ 0 & \Phi_B & 0 & 0 \\ 0 & 0 & \Phi_C & 0 \\ 0 & 0 & 0 & \Phi_{TS} \end{bmatrix} Lq_g \tag{8}$$

## 4. Substructuring Results

The experimental single-blade-and- hub system was used in the substructuinrg calculations detailed in the previous section to create a full hub-and-three-bladed turbine model. This substructured model will now be now compared to the results from the truth test described earlier in this paper. Because some modes of the system were found to be closely spaced these modes had to be correlated based on their Modal Assurance Criterion (MAC) values. This identification was important when looking at the 8th and 9th substructured modes as well as the 13th and 14th. These modes could be identified by MAC values as well as visual representation The MAC values and modal parameter comparisons can be seen in Table 5.

| Truth Mode | Frequency (Hz) | Damping Ratio | Substr. Mode | Substr. Frequency (Hz) | Frequency Error | Substr. Damping | Damping Error | MAC |
|---|---|---|---|---|---|---|---|---|
| 7 | 20.56 | 1.00% | 7 | 23.49 | 14.26% | 0.73% | -27.19% | .9912 |
| 8 | 27.78 | 0.98% | 9 | 28.33 | 2.00% | 0.86% | -12.07% | .7655 |
| 9 | 29.03 | 0.87% | 8 | 28.03 | -3.44% | 0.85% | -1.88% | .8808 |
| 10 | 61.10 | 1.71% | 10 | 66.53 | 8.91% | 0.71% | -58.31% | .9422 |
| 11 | 64.29 | 1.27% | 11 | 66.67 | 3.72% | 0.71% | -44.03% | .9787 |
| 12 | 70.68 | 1.11% | 12 | 77.33 | 9.41% | 0.84% | -23.71% | .9402 |
| 13 | 99.40 | 1.48% | 14 | 96.30 | -1.75% | 1.00% | -32.17% | .8618 |
| 14 | 102.95 | 1.08% | 13 | 97.66 | -6.45% | 0.99% | -8.82% | .8849 |
| 15 | 155.00 | 1.33% | 15 | 167.26 | 7.91% | 1.29% | -3.05% | .7850 |

**Table 5. Substructuring Results**

By inspection of Table 5, some trends can be identified. The first, second and third in-phase out-of-plane bending modes (Modes 7, 12 and 15) are too high in frequency. Three of the four anti-symmetric out of plane bending modes (9, 13 and 14) are low in frequency. The edgewise modes (10 and 11) are high in frequency.

The substructured damping ratios are a further off than the natural frequencies. Some modes (9 and 15) are quite close in damping while others are as high as 58% off mark.

The correlation of modes between the substructured and truth models could be determined either by MAC (Figure 9) or visual comparison (Figures 10 and 11). Figure 8 contains the bending modes in an isometric view while Figure 9 shows the edgewise modes in the *xy* plane.

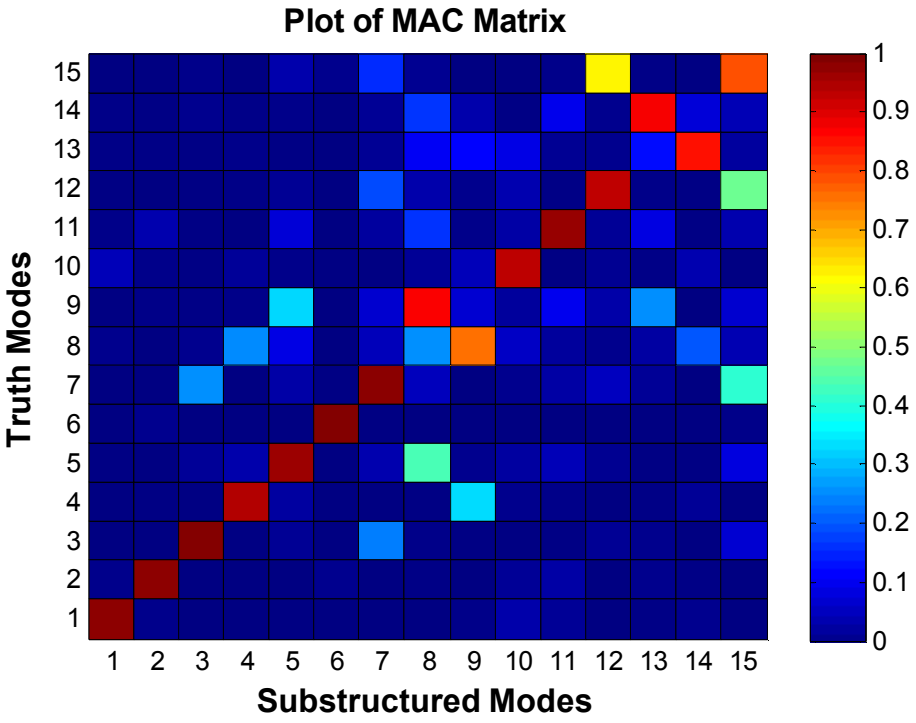


**Figure 7. MAC between Truth and Substructured modes**

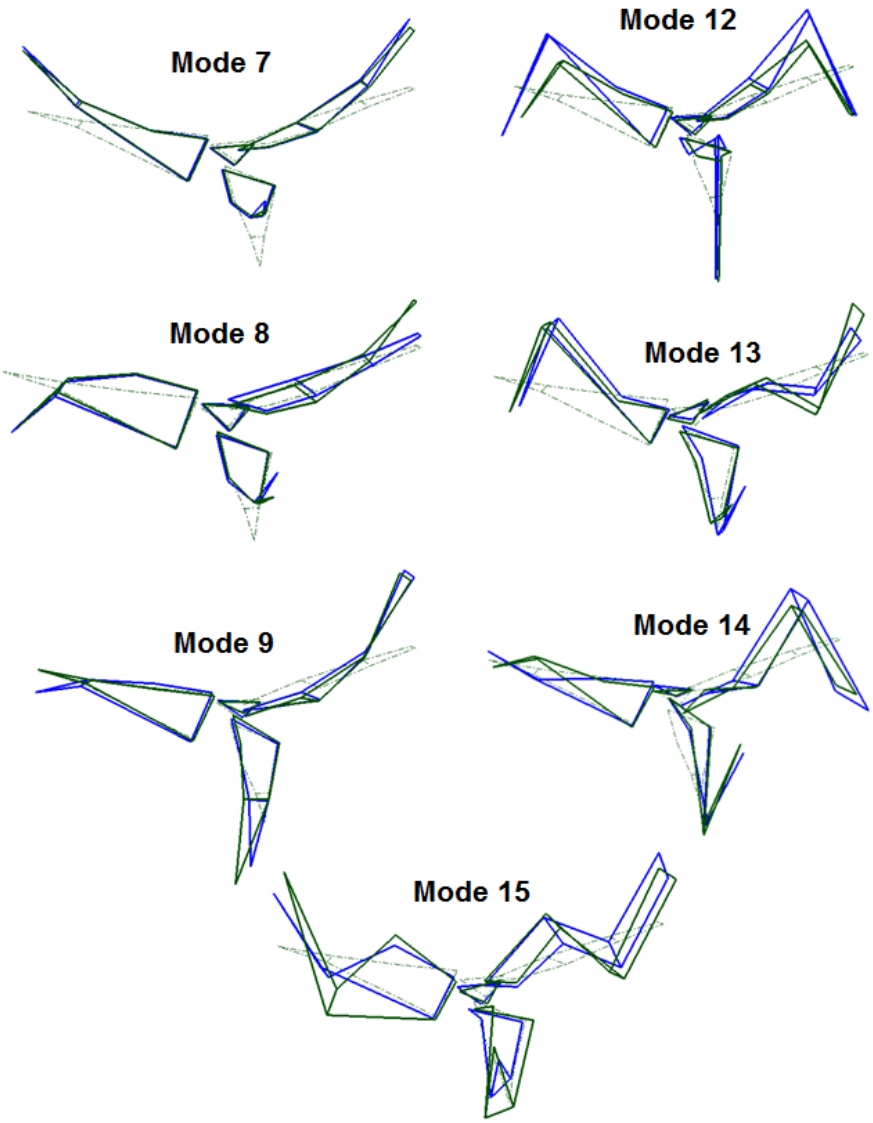


**Figure 8. Bending mode shape comparison (Blue – Substructured, Green – Truth Test, Dashed – Undeformed)**

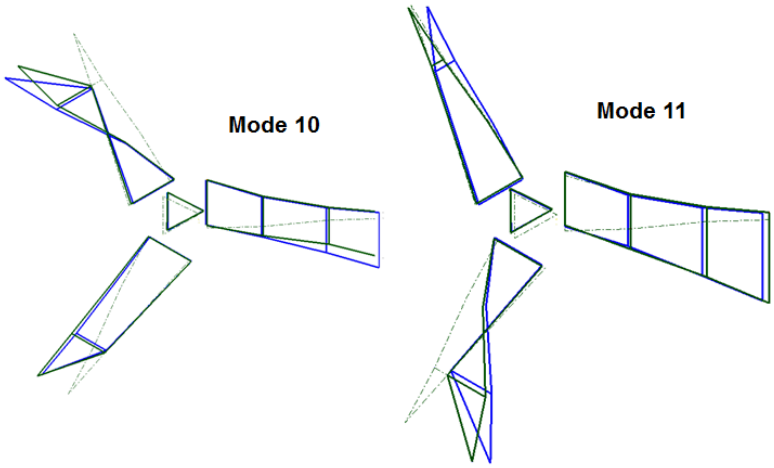


**Figure 9. Edgewise mode shape comparison (Blue – Substructured, Green – Truth Test, Dashed – Undeformed)**

## 5. Possible Error Sources

There were errors of up to 15% in natural frequency, 59% in damping and MAC values as low as 0.7655. Several issues could lead to these errors that could be investigated further with additional study. Some important experimental check and possible error sources will be mentioned in this section. Modal truncation errors are known to exist but they are not addressed in this exercise.

### 5.1 Testing Checks and Validations

Previous work [7] has shown that the most important mode shapes to obtain accurately are the rigid body mode shapes. When analytically adding rigid body modes to the experimental data, a check can be performed to ensure the analytically derived rigid body modes are a good match of the system that was tested. In this case, we can take the derived rigid body mode FRF and overlay the plot with the driving point FRF taken from experimental data. Rigid body modes are often hard to extract, but the masslines of these rigid body modes can be compared in such a plot. Figure 10 shows a massline comparison for our substructure. After the rigid body modes, around 1-2 Hz, the massline magnitude should be similar between the analytical and measured FRFs. If this is not true, the mass properties used to calculate the rigid body modes may be off and could be adjusted to get a better model of the system.

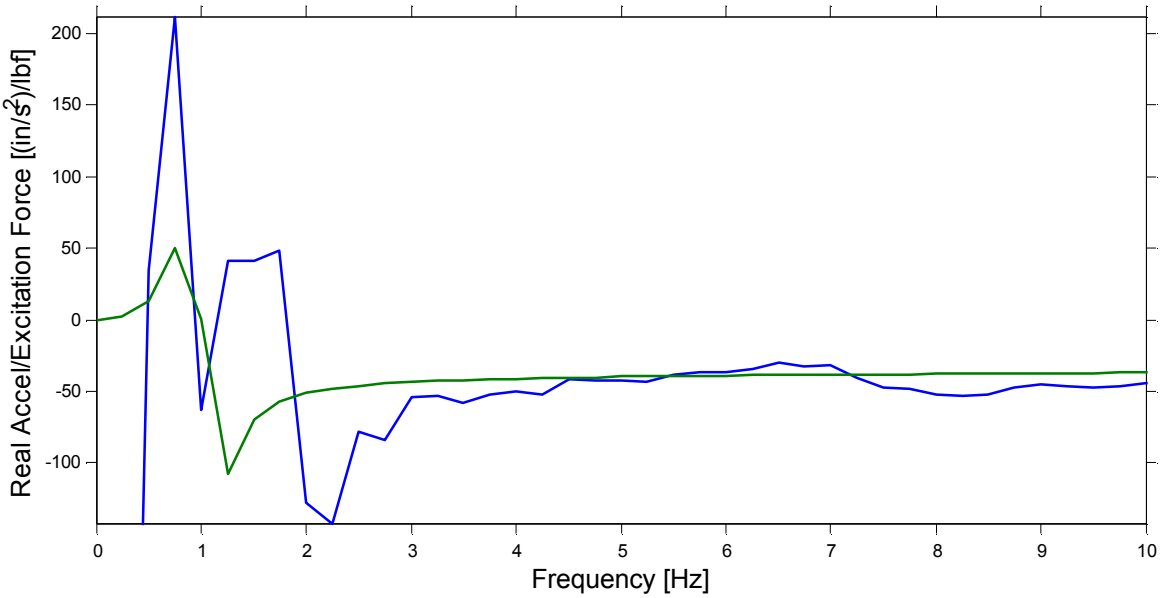


**Figure 10. Rigid Body Massline Comparison: Blue – Measured Data, Green – Analytical Model**

Additional best practices were followed when setting up and performing the experiments. Hammer calibration lab reports showed up to 15% variation of hammer measurement sensitivity. To mitigate this large error source the hammer sensitivity was adjusted using a large block of known mass with a high sensitivity accelerometer attached. The hammer sensitivity was adjusted and checked to within accelerometer specified accuracy.

Also, as mentioned previously, multiple reference locations were used. In the final model the best fit for each elastic mode shape was utilized. The red circles in Figure 6 show which reference locations provided the best fit for each elastic mode.

### 5.2 Transmission Simulator Stiffness

This exercise was completed assuming the transmission simulator was completely rigid and therefore only the rigid body modes of the transmission simulator were used. The flanges were mounted on a shaft that extends into a mechanism within the hub. This mechanism was potted, but it was observed that small amounts of flexibility may still be present. Ignoring this flexibility means the transmission simulator model was too stiff and may have led to the increased natural frequencies as seen in modes that strain this potting the most.

### 5.3 Accelerometer Mounting

The accelerometers used on the rotor hub and Blade A were not removed between the testing of the hub-and-three-bladed and single-blade-and-hub systems. Therefore, they are in the same position from test to test. Blades B and C were instrumented

individually for the hub-and-three-bladed test. Small discrepancies were found in the placement of the accelerometers on Blades B and C when compared to those of Blade A. These deviations on the order of one-eighth of an inch could lead to errors when results from Blade A are rotated and assumed to be in the same locations but in the Blade B and C coordinate systems. An additional substructuring exercise was completed using the six degrees of freedom of the center of mass of the hub as the connection degrees of freedom to abate these measurement discrepancies. This method led to a small change in natural frequency (less than 2%).

### 5.4 Damping Errors

Calculated damping ratios had the highest errors. When assembling the system the damping is all placed on the diagonal of the damping matrix when in reality there are coupled terms within the damping matrix. Neglecting these coupled terms makes the mathematics simpler but leads to less accurate results than desired. Further investigation would be warranted to attempt to include these coupled damping terms in the substructuring process.

## 6. Conclusions and Future Work

This exercise used an experiment on a single-blade-and-hub substructure to create a model of a full hub-and-three-bladed assembly. This substructure was rotated and linked together generating three blades and three hubs (transmission simulators), thus two of the hubs were analytically removed. The results of this substructuring exercise were then compared to an experiment conducted on the full hub-and-three-bladed assembly. The rigid body modes for these cases were constructed from mass properties.

After substructuring, all elastic modes could be correlated to the truth model either through MACs or using visual shapes. The worst frequency error was about 15 percent in the first mode. The damping ratios were the most difficult to predict with error as high as 55%. MAC values ranged from 0.77 to 0.99. Future work to improve these measurements could be completed by measuring the elastic modes of the transmission simulator by mass loading the flanges and completing another substructuring exercise. Further investigation of the system damping to include the coupling terms may also be of interest to look at improving substructure modal damping ratio predictions.

**References**


[1] R.L. Mayes and M. Arviso, "Design Studies for the Transmission Simulator Method of Experimental Dynamic Substructuring," *International Seminar on Modal Analysis 2010,* Lueven, Belgium, 2010.

[2] R.L Mayes, "An Introduction to the SEM Substructures Focus Group Test Bed – The Ampair 600 Wind Turbine", *Proceedings of the 30th International Modal Analysis Conference,* Orlando, Florida, February 2012.

[3] D. P. Rohe. and R. L. Mayes, "Coupling of a Bladed Hub to the Tower of the Ampair 600 Wind Turbine using the Transmission Simulator Method.", *Proceedings of the 31st International Modal Analysis Conference,* Garden Grove, California, February 2013.

[4] J. Gross, T. Oberhardt, P. Ruess, and L .Gaul, "Model Updating of the Ampair Wind Turbine Substructures.", *Proceedings of the 32nd International Modal Analysis Conference*, Orlando, Florida, February 2013.

[5] D. P .Hensley, and R. L. Maye, "Extending SMAC to Multiple References", *Proceedings of the 24th International Modal Analysis Conference*, pp.220-230, February 2006.

[6] T. G. Carne, D. T. Griffith, and M. E. Casias, "Support Conditions for Experimental Modal Analysis." *Sound and Vibration*, Vol. 41 (2007), pp. 10-16.

[7] D. P. Rohe and M. S. Allen, "Investigation into the Effect of Mode Shape Errors on Validation Experiments for Experimental-Analytical Substructuring*", Proceedings of the ASME 2012 International Design Engineering Technical Conferences & Computer and Information in Engineering Conference,* Chicago, Illinois, August, 2012.